Journal of Hydrology 579 (2019) 124194

Contents lists available at ScienceDirect

Journal of Hydrology

journal homepage: www.elsevier.com/locate/jhydrol

Research papers

The relative contributions of precipitation, evapotranspiration, and runoff to terrestrial water storage changes across 168 river basins

Yafeng Zhang[a], Bin He[a,*], Lanlan Guo[b], Junjie Liu[a], Xiaoming Xie[a]

[a] State Key Laboratory of Earth Surface Processes and Resource Ecology, College of Global Change and Earth System Science, Beijing Normal University, Beijing 100875, China

[b] Academy of Disaster Reduction and Emergency Management, School of Geography, Beijing Normal University, Beijing 100875, China

ARTICLE INFO

This manuscript was handled by Marco Borga, Editor-in-Chief, with the assistance of Di Long, Associate Editor

Keywords:
GRACE
TWSC
Precipitation
Evapotranspiration
Contribution

ABSTRACT

Changes of global terrestrial water storage (TWS) retrieved from the Gravity Recovery and Climate Experiment (GRACE) satellite mission have been extensively evaluated in previous studies. However, natural drivers and their relative contributions to global TWS changes (TWSC) are still poorly understood. In this study, based on two global precipitation (P) datasets, three global evapotranspiration (ET) datasets, and one global runoff (R) dataset, the responses of TWSC to the three major water fluxes, P, ET, and R, were comprehensively examined for 168 river basins. In addition, by using hierarchical partitioning (HP) analysis, the corresponding relative contributions (RC) of P, ET, and R to TWSC were quantified. The results showed that for the period Jan. 2003–Dec. 2011, significant increases in terrestrial water storage anomalies (TWSA) were observed over 49 basins, whereas 42 basins presented significant decreases in TWSA. A robust positive relationship between P and TWSC was observed in low-latitude basins, but strong negative relationships of TWSC with ET and R were identified in mid- and high-latitude basins. Averaging the degree of explanation of 168 basins for all P–ET–R combinations, we found that three independent variables explained an average of 61.4% of TWSC. The corresponding RC of P, ET, and R were 42.6%, 43.2% and 4.2%, respectively. In spatial terms, a larger contribution of P to TWSC was found in low-latitude basins, and larger contributions of ET and R were identified for mid-and high-latitude basins. The findings of this study were important for improving our understanding of global TWSC responses to climate change.

1. Introduction

Terrestrial water storage (TWS) reflects all types of water stored on continents, including surface water, soil water, glaciers, and groundwater etc. (Pokhrel et al., 2012a; Tregoning et al., 2012; Yun et al., 2017). Variations in TWS have large impacts on terrestrial ecosystems, human beings, and even the sea level (Deng and Chen, 2016). Climate change and human activities have changed both the magnitude and spatial distribution of TWS (Pokhrel et al., 2012b). TWS monitoring and the investigation of its attributes are therefore crucial for water resource management and sustainable utilization.

Observations made by the Gravity Recovery and Climate Experiment (GRACE) satellite mission have provided integrated and accurate measurements in global TWS anomalies since April 2002 (Tapley et al., 2004a,b). By this dataset, global and regional TWS changes (TWSC) and its relationships with various climatic variables have been investigated. For example, Based on GRACE data and model output for 30 basins, Felfelani et al. (2017) investigated the component contribution ratios of snow water, surface water and subsurface water to TWSC. Asoka et al. (2017) explored features of groundwater storage changes in India and highlighted the dominant influence of monsoon precipitation. Similar studies have also been conducted in Africa to determine natural and anthropogenic influences on TWSC (Ahmed et al., 2014). Strong anthropogenic influences (Tang et al., 2013) and the impacts of climate extremes (flood and drought) on TWSC have also been evaluated in depth (Khandu et al., 2016, 2015; Leblanc et al., 2009; Long et al., 2013). However, a global examination of drivers and their contributions to TWSC is still lacked.

Precipitation (P), as the main input flux of terrestrial water, together with evapotranspiration (ET) and runoff (R), as two main output fluxes, play key roles in the global water cycles (Oki and Kanae, 2006; Thomas, 2006). Ignoring anthropogenic influences, these three hydrological fluxes theoretically dominant global TWSC (Rodell et al., 2004; Syed et al., 2008). Some studies have attempted to reveal their relationships

* Corresponding author.
E-mail address: Hebin@bnu.edu.cn (B. He).

https://doi.org/10.1016/j.jhydrol.2019.124194
Received 27 June 2019; Received in revised form 20 September 2019; Accepted 27 September 2019
Available online 28 September 2019
0022-1694/

with TWSC at various scales. Syed et al. (2008) evaluated the temporal and spatial characteristics of Global Land Data Assimilation System (GLDAS) based TWSC and explored the relationship of P, ET and R on GLDAS based TWSC. They found that the positive correlation between P and TWSC occurred in the low latitude, and the relationships of ET, R and TWSC were negative in the middle and high latitude, respectively. Mo et al. (2016) explored the temporal variation of GRACE based TWSC in China, and suggested that changes in P, ET and R contribute 46%, 41% and 32% to TWSC from 2003 to 2013, respectively. Soni and Syed (2015) evaluated the relationship of the hydrologic flux and TWSC variation over the four river basins (Ganga, Godavari, Krishna and Mahanadi basins) in India. They found that the P minus ET played an important role in the TWSC variation. After considering the flux individually, they found that P dominated the TWSC over the basins. Currents studies either qualitatively investigated the relationships of TWSC with hydrological fluxes at global scale, or quantitatively determined their relationships at regional or basin scale. Few of these studies have quantified the relative contributions of hydrological fluxes to TWSC at a global scale, which is critical for understanding TWSC under a changing climate.

The aims of this study are to examine the responses of TWSC to precipitation (P), evapotranspiration (ET), and runoff (R) in the global 168 major river basins and to quantify the relative contributions of P, ET, and R to TWSC in each basin based on hierarchical partitioning (HP) analysis. To reduce the uncertainties associated with datasets, two P datasets, three ET datasets, and one observed R dataset were analyzed here, as listed in Table 1. The performances of different combinations of P–ET–R datasets in explaining TWSC were also evaluated and compared.

2. Materials and methods

2.1. Study regions

In this study, 168 major river basins, covering 66×10^6 km^2 of global continents, were selected here for analysis. According to Scanlon et al. (2017), the criteria for basin selection are that 1) basin area is > 40,000 km^2 and 2) basin radius is > 200 km. The digital map of the 168 river basins was obtained from the Global Runoff Data Centre (GRDC; http://grdc.bafg.de) (Fig. 1). In addition, following the aridity classification of the United Nations Environment Programme, the aridity of each basin was determined by calculating the ratio of 30 yr (1982–2011) mean P and mean potential evapotranspiration (PET) (Feng and Fu, 2013) (Fig. 1). The P and PET datasets were obtained from the Climate Research Union (CRU). PET was calculated by the Penman Equation (Saylor, 1992).

2.2. Data

2.2.1. GRACE data

The newly released GRACE level–2 Mascon solutions produced by NASA's Jet Propulsion Laboratory (JPL) and the Center for Space Research (CSR) at the University of Texas were used here to estimate the monthly TWS anomalies (TWSA). The CSR Mascon solution, calculated on equal–area geodesic grids of about 120 km (1° at the equator), is processed by constraining the original GRACE level–1 data through the Tikhonov regularization method that effectively depresses the north-south stripe errors (Save et al., 2016), and is presented on 0.5° × 0.5° grids. The JPL Mascon data are constrained by both GRACE data and a priori information obtained from the near-global geophysical models, obtaining the same effect of suppressing corresponding errors (Watkins et al., 2015). Using downscaling factors calculated by the Community Land Model (CLM ver. 4.0), the coarse 3° × 3° JPL Mascon data is then downscaled to 1° × 1° and resampled to 0.5° × 0.5°. Detailed descriptions of approaches to processing CSR and JPL Mascon products can be found in studies by Watkins et al. (2015) and Save et al. (2016). Here, the monthly TWSA series from Jan. 2003 to Dec. 2011 was averaged from JPL Mascon and CSR Mascon. Missing records for several months were replaced by averaging the values of adjacent months (Andrew et al., 2017; Long et al., 2015; Mo et al., 2016).

2.2.2. Precipitation

Two monthly P datasets were used for analysis, obtained from the Climatic Research Unit (CRU) (http://data.ceda.ac.uk//badc/cru/) Time–Series Version 4.00 (defined as P_{CRU}) and the Global Precipitation Climatology Centre (GPCC) (https://www.esrl.noaa.gov/psd/data/gridded/data.gpcc.html) (defined as P_{GPCC}), respectively. The P_{CRU} dataset provides global 0.5° month-by-month precipitation data for the period 1901–2014 (Harris et al., 2014). The 0.5° P_{GPCC} dataset during 1901–2013 was produced by compiling monthly precipitation observations from more than 70,000 stations across the world (Schneider et al., 2014).

2.2.3. Evapotranspiration

In situ ET observations can be obtained only from individual stations or regional studies. Therefore, large–scale ET investigations still rely on estimations from satellite observations or simulations from land surface models. In this study, ET of river basins was derived from three datasets: (1) the Moderate Resolution Imaging Spectroradiometer (MODIS) ET product (MOD16A2) (http://files.ntsg.umt.edu/data/NTSG_Products/MOD16/), (2) ET estimations produced by Jung et al. (2009) based on in–situ FLUXNET observations (https://www.bgcjena.mpg.de/geodb/projects/FileDetails.php), and (3) ET products

Table 1
Datasets used in this study.

Variables	Product	Temporal resolution	Spatial resolution	Periods
Terrestrial Water Storage (TWS)	GRACE RL05 Mascon Solutions (CSR)	Monthly	0.5°	Apr. 2002–Jun. 2017
	GRACE RL05 Mascon Solutions (JPL)	Monthly	0.5°	Apr. 2002–Jun. 2016
Soil moisture storage (SMS)	Global Land Data Assimilation System	Monthly	1°	1979–2019
Canopy water storage (CWS)		Monthly	1°	1979–2019
Snow water equivalent (SWE)		Monthly	1°	1979–2019
Surface water storage (SWS)		Monthly	1°	1979–2019
Precipitation (P)	CRU time series, TS 4.00 (P_{CRU})	Monthly	0.5°	1901–2014
	Global Precipitation Climatology Centre (P_{GPCC})	Monthly	0.5°	1901–2013
Evapotranspiration (ET)	MOD16A2(ET_{MODIS})	Monthly	0.5°	2000–2014
	ET_{Jung}	Monthly	0.5°	1982–2011
	Global Land Data Assimilation System (ET_{GLDAS})	Monthly	1°	1979–2019
PET	CRU time series, TS 4.00	Monthly	0.5°	1901–2014
Runoff	Dai (2016)	Monthly	Basin scale	1901–2014
Global basins database	GRDC	Shape files		

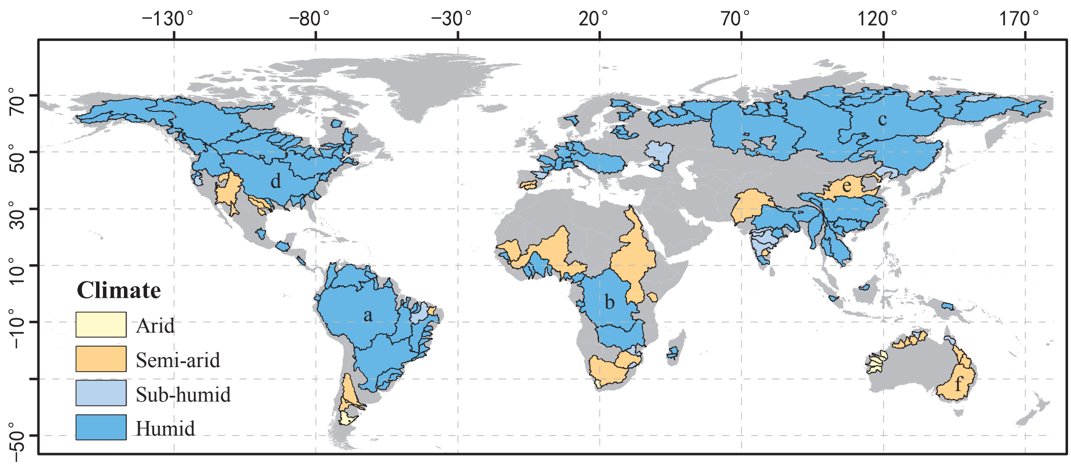

Fig. 1. Distribution of the selected river basins and corresponding climate. a–f indicate the basins selected as case studies (a, Amazon; b, Congo; c, Lena; d, Mississippi River; e, Yangtze River; f, Murray).

simulated by the Noah, VIC, CLM and Mosaic models, with forcing by GLDAS 1.0 (https://hydro1.gesdisc.eosdis.nasa.gov/data/GLDAS/). The three ET products are identified using the following subscripts: ET_{MODIS}, ET_{Jung}, and ET_{GLDAS}.

The ET_{MODIS} product with a spatial resolution of 0.5° was estimated using the Penman–Monteith equation (Mu et al., 2011), with inputs from MODIS retrievals, and provides global monthly ET values from 2000 to 2014. This product has been widely used in research on land surface ecological and hydrological processes (Luus et al., 2013; Mishra et al., 2015). The global 0.5° ET_{Jung} product covering the period 1982 to 2011 was simulated through a machine learning method, the model tree ensemble, which is trained with global in-situ FLUXNET observations (Jung et al., 2009). Based on this dataset, Jung et al. (2010) investigated the global trend and attributes of ET.

GLDAS provides monthly ET simulations from 1979 to present. The global 1° ET_{GLDAS} data were averaged from outputs of Noah, VIC, CLM and Mosaic models, covering the period 2003 to 2011. The accuracy of the ET_{GLDAS} has been validated by several studies. For example, Khan et al. (2018) evaluated the uncertainties in ET based on GLEAM, GLDAS, and MOD16. They found that the three products exhibited reasonable accuracy compared with in–situ actual evapotranspiration within Asia. Rodell et al. (2004) compared global ET datasets by classifying them into four categories: (1) diagnostic datasets, (2) LSM datasets, (3) reanalysis datasets, and (4) IPCC AR4 datasets. The results revealed that the patterns of mean values are highly congruent across all categories.

2.2.4. Runoff

The long-term observed runoff data were obtained from GRDC. As the majority of basins suffer some proportion of missing data, the simple method proposed by Dai (2016) was used to fill data gaps. Correlations were firstly calculated between observed runoff and precipitation, model-simulated runoff, and the Palmer Drought Severity Index. Whichever showed the highest correlation coefficient was then used to fill gaps in the observed runoff data using linear regression. In total, runoff data for 168 basins were available for the study period (Jan. 2003–Dec. 2011) (Ozdogan et al., 2010; Sneeuw et al., 2014).

Considering the data availability for all datasets, the period of Jan. 2003–Dec. 2011 was selected for analysis in this study.

2.3. Methods

2.3.1. Calculation of TWSC

The water balance equation in a given basin can be expressed as follows:

$$\frac{ds}{dt} = \sum_{t-1}^{t} P - \sum_{t-1}^{t} ET - \sum_{t-1}^{t} R \tag{1}$$

where s is total water storage, $\frac{ds}{dt}$ is TWSC for a specific period (t), P is precipitation, ET is actual evapotranspiration, and R is runoff. According to Eq. (1), it is clear that TWSC is determined by changes in P, ET, and R. For comparison, TWSC was also calculated by water balance equation here ($TWSC_{P\text{-}ET\text{-}R}$).

TWSA refers to the residual storage at a given time with respect to the storage at a reference time (Rodell et al., 2009). In addition to the GRACE based TWSA, the performance of GLDAS based TWSA was also investigated in this study. The GLDAS based TWSA was calculated as the sum of the anomalies of individual components, such as Canopy water storage anomalies (CWSA), Soil moisture storage anomalies (SMSA), Snow water equivalent anomalies (SWEA) and Surface water storage anomalies (SWSA), which were determined as the difference of Canopy water storage (CWS), Soil moisture storage (SMS), Snow water equivalent (SWE) and Surface water storage (SWS) and the corresponding the average of CWS, SMS, SWE and SWS for the period January 2003 to December 2011, respectively.

The difference of TWSA at the two joint time is named as TWSC (Moiwo et al., 2012, 2011). Here, the double–difference derivation of GRACE based TWSA and GLDAS based TWSA were used to estimate TWSC derived from GRACE and GLDAS based TWSC at a monthly scale (cm/month) (Long et al., 2014), respectively, as follows:

$$TWSC = \frac{ds}{dt} \approx \frac{dTWSA}{dt} \approx \frac{TWSA(t+1) - TWSA(t-1)}{2\Delta t} \tag{2}$$

2.3.2. Trend analysis

As a common non-parametric test, the Mann–Kendall rank-based test is used here to detect trends for TWSC time series (Humphrey et al., 2016). This method, proposed by Mann (1945) and improved by Kendall (1975), has frequently been used in trend analysis of hydrological and meteorological variables (Aziz and Burn, 2006; Burn and Elnur, 2002; Gocic and Trajkovic, 2013). The significance of TWSC trends was evaluated at $p < 0.05$.

2.3.3. Partial correlation analysis and autocorrelation test

The response of TWSC to P, ET, and R was examined by partial correlation analysis, which excludes the influence of other factors on correlations between two variables. The significance of correlations was evaluated at $p < 0.05$. Before running the correlation analysis, Durbin–Watson statistics (Durbin and Watson, 1971) were used to test for temporal autocorrelation in the P, ET, R, and TWSC time series, and then the first-order difference method was applied to eliminate autocorrelations (Anderson, 1942).

2.3.4. Hierarchical partitioning analysis

HP analysis proposed by Chevan and Sutherland (1991) was used here to quantify the relative contributions of P, ET, and R on TWSC. Compared to common methods for determining variable importance using a single-model, HP measures the importance of each independent variable with respect to the dependent variable as a percentage contribution to the goodness-of-fit of the multivariate linear regression model. Hence, it is suggested to provide a robust assessment of variable importance and can effectively overcome the collinearity problem existing among two or more explanatory variables. The theory of HP can be expressed by the following equation (Chevan and Sutherland, 1991):

$$\sum_{b=1}^{N} r_b = \sum_{b=1}^{N} I_b + \sum_{b=1}^{N} J_b \tag{3}$$

where r is the goodness-of-fit between dependent and independent variables in regression analysis; I and J are the independent and joint components of r, respectively; and N is the number of independent variables. In regression analysis, for any independent variable such as m, $r_m = I_m + J_m$, I_m refers to that part of the percentage of the degree of fitting of m to dependent variables, whereas J_m refers to the remaining percentage of the degree of fitting of m to other independent variables (Chevan and Sutherland, 1991). The HP analysis was carried out with R software. As two P datasets and three ET datasets were available, HP analysis was performed between TWSC and six different P–ET–R combinations.

2.3.5. Estimation of uncertainties

TWSA errors in the JPL dataset can be attributed to measurement errors and leakage errors, which have been provided in associated products. Errors in the CSR dataset are considered to be the TWSA residuals after the long–term, annual, and semiannual trends have been removed from the original signal (Scanlon et al., 2017). Standard linear least–squares regression was applied to decompose the long–term, annual, and semiannual trends from the original signal, details of which can be found in Wahr et al. (2006) and Hirsch and Slack (1984). The uncertainty in TWSC is calculated from TWSA according to the error propagation law in Eq. (1) (Rodell et al., 2004). Details about estimates of uncertainties can be found in Wahr et al. (2006) and Wiese et al. (2016). Uncertainties in the three ET datasets, two P datasets, and TWSC data from two GRACE products were estimated as the standard deviations (Longuevergne et al., 2010; Pan et al., 2017; Yang et al., 2015).

3. Results

3.1. Response of TWSC to precipitation, evapotranspiration and runoff

Fig. 2 shows the trend in TWSA variations for the period of Jan. 2003–Dec. 2011 for 168 river basins. A total of 49 basins ($p < 0.05$) shown significant increasing trends, including the Yangtze, Mississippi and Yenisei basins, etc. In contrast, significant decreases in TWSA ($p < 0.05$) were observed in 42 basins, such as the Yellow River, Ganges and Indus basins. This pattern was similar to that reported by, Rodell et al. (2018), Long et al. (2017), Reager et al. (2016) and Scanlon et al. (2016), etc. In addition, it was reasonably consistent with some regional-scale investigations (Ahmed et al., 2014; Asoka et al., 2017; Tang et al., 2013).

Then, the responses of TWSC to P, ET and R were determined using partial correlation analysis. Before this analysis, the temporal autocorrelation in the time series of TWSC, P, ET, and R was first tested. Significant first-order auto-correlations were observed for all time series, indicating potential impacts on the results of correlation analysis. After eliminating auto-correlations by the first-order difference method, partial correlations between TWSC, P, ET, and R for the period Jan. 2003–Dec. 2011 were calculated basin by basin. The distributions of correlation coefficients between TWSC and P presented similar patterns with different P-ET-R combinations (Figs. 3a, S1–S3). Consistent with Syed et al. (2008), a general positive relationship was observed between TWSC and P for most basins. Most basins in low latitudes showed strong positive correlations, including the Amazon, Congo, and Nile basins, etc. Weaker relationships were observed in mid-latitude and high-latitude basins. The mean partial correlation coefficient of all TWSC–P combinations for all the basins was 0.523 ± 0.024.

Significant negative correlations between TWSC and ET were shown in most mid-and high-latitude basins, especially for the Northern America (Figs. 3b, S1–S3), such as the Mississippi and Yenisei basins. However, in the lower–latitude basins, weak positive relationships were observed, such as in the Amazon basin and Congo basin, etc. The average correlation coefficient between TWSC and the three ET datasets for the basins was -0.401 ± 0.043. A general negative relationship between TWSC and R was observed over most basins, and strong negative relationships were identified in the northern high latitudes (Figs. 3c, S1–S3). Interestingly, we also found that negative correlation coefficients between TWSC and R in basins of northern Asia are larger than those in Northern America. According to the water balance equation (Eq.1), a negative relationship between TWSC and R can be expected. However, positive relationships were also observed in some low latitude basins, such as the Congo basin, Murray basin, Indus basin and Ganges basin. Although this phenomenon has been reported by previous studies (Frappart et al., 2013; Soni and Syed, 2015), few of them had provided the reasons. We speculated this abnormal TWSC-R relationship should be induced by 1) human associated activities, such as irrigation practices, construction of channels and dams, etc., which disrupt water balance within basins; 2) influences from other water fluxes, such as snowmelt, which cause the covariation of TWSC and R; 3) uncertainties caused by datasets, for example, P_{CRU}-ET_{Jung}-R combination suggested a higher stronger positive relationship for TWSC and R than that of P_{GPCC}-ET_{MODIS}-R combination.

To test the potential uncertainty of correlation analysis caused by the choice of lengths of time sequence, we also performed the partial correlation analysis for the periods Jan. 2003–Dec. 2009 (Figs. S4–S6 and Table S1) and Jan. 2005–Dec. 2011 (Figs. S7–S9; and Table S1). Although these periods differ, comparable correlation coefficients and patterns were obtained for most of the basins, confirming the basic relationships of TWSC with P, ET, and R established in this study.

3.2. The relative contributions of precipitation, evapotranspiration, and runoff to TWSC

Based on the HP analysis, the relative contributions of P, ET, and R to TWSC were determined for each basin for different P–ET–R dataset combinations. Table 2 lists all values of averaged explained variance (r^2) for multivariate regression models of different P–ET–R combinations as well as the corresponding independent contributions of P, ET, and R to TWSC. In spite of the marked differences between the data sources, the six models built from different P–ET–R combinations present comparable values of r^2, approximately 0.614 ± 0.024, suggesting the relatively strong performance of models in explaining TWSC. The maximum r^2 value (0.638) was given by the model built between TWSC and P_{GPCC}–ET_{Jung}–R combination. In addition, the spatial distributions of r^2 for each model show similar patterns (Figs. 4 and S10). The higher values of r^2 were concentrated in several low-latitude basins, such as the Amazon, Nile, Parana, Yangtze, and Congo river basins, whereas relatively low values of r^2 were observed in high-latitude basins, such as the Mississippi basin and Lena basin, etc.

In addition, the r^2 and the relative contribution of P, ET and R to GLDAS based TWSC were also quantified (Figs. S14–S17). The spatial pattern of the degree of explanations of P, ET, and R to GLDAS based TWSC (Fig. S14) were similar to that of TWSC derived from GRACE

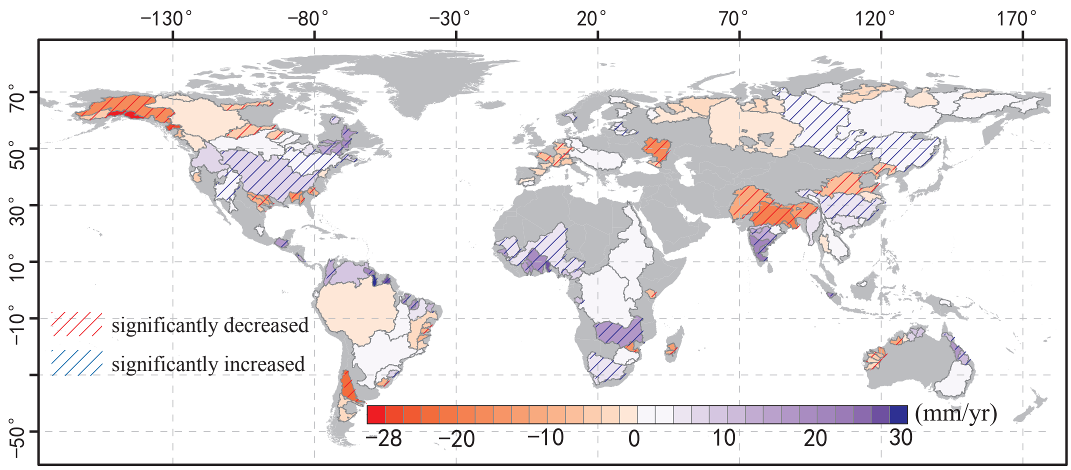

Fig. 2. The trend of TWSA variations for the 168 analyzed basins.

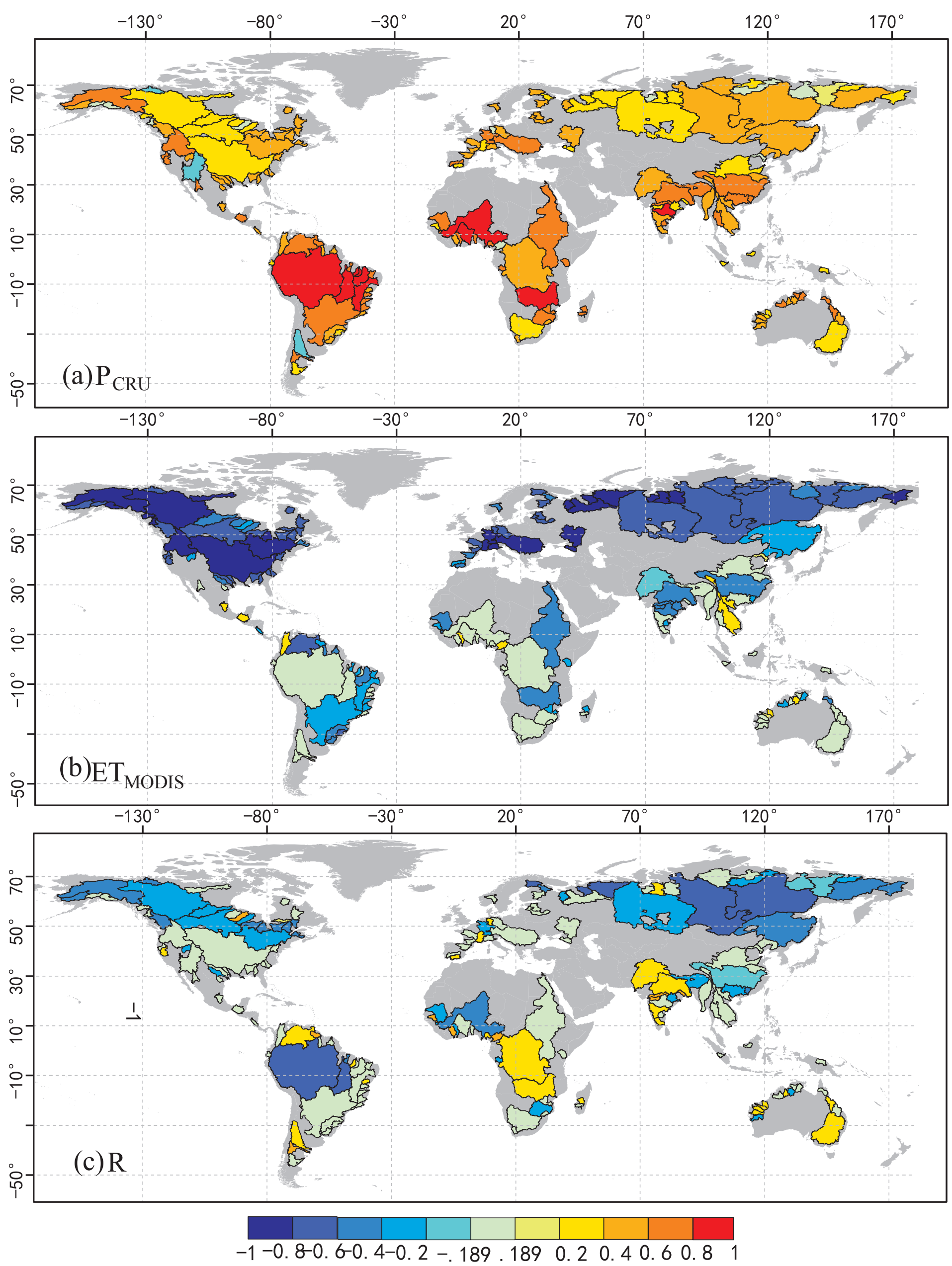

Fig. 3. Partial correlations of TWSC with P (a), ET_{MODIS} (b), and R (c). Correlation coefficient of ± 0.189 indicates a significance level of 0.05.

Table 2
Results of HP analysis with different combinations of P, ET and R datasets.

P-ET-R combinations	r^2	RC of P (%)	RC of ET (%)	RC of R (%)
P_{CRU}-ET_{MODIS}-R	0.620	42.7	40.8	16.5
P_{CRU}-ET_{Jung}-R	0.637	38.9	46.9	13.3
P_{CRU}-ET_{GLDAS}-R	0.589	45.4	42.3	12.3
P_{GPCC}-ET_{MODIS}-R	0.620	43.3	40.5	16.2
P_{GPCC}-ET_{Jung}-R	0.638	39.7	46.2	14.1
P_{GPCC}-ET_{GLDAS}-R	0.580	45.6	42.3	12.1
Average	0.614 ± 0.024	42.6 ± 2.81	43.2 ± 2.7	14.2 ± 1.9

(Figs. 4 and S10), but the averaged degree of explanation ($r^2 = 0.631 \pm 0.05$) was slightly higher than the later over global 168 basins. This is not surprising because GLDAS based TWSC is estimated strictly following the water balance equation, and incorporates climate and vegetation information overlapping with datasets used in this study. After differencing the r^2 of GRACE based TWSC and GLDAS based TWSC (Fig. S18), we also found that the r^2 of GLDAS based TWSC was underestimated in some basins, such as the Congo basin, Indus basin, Ganges basin and the northern of Mississippi basin, etc. It may be related to the absence of ground water storage in GLDAS LSMs (Scanlon et al., 2019; Syed et al., 2008) or the uncertainties of GLDAS caused by deficits of LSMs or uncertainties of climate forcing data (Syed et al., 2008).

For all 168 basins, the average relative contributions of all P-ET-R combination to GRACE based TWSC were 42.6% ± 2.81%, 43.2% ± 2.7%, and 14.2% ± 1.9%, respectively. The similar spatial patterns were shown for different P-ET-R combinations (Figs. 5, S11–S13). Taking P_{CRU}-ET_{MODIS}-R as an example (Fig. 5), we found that P has a larger contribution in low-latitude basins, especially in tropical basins, such as the Amazon and Congo river basins. In contrast, a larger contribution of ET was identified in mid and high latitudes, such as for the Mississippi, Mackenzie, Yenisei, and Lena river basins. Compared with P and ET, R has a smaller contribution to TWSC. A larger contribution of R was identified in mid and high latitudes than in low latitudes, especially for the Yenisei, Lena, and Ob basins. An interesting phenomenon was that although larger contributions of ET and R to TWSC are observed in mid and high latitudes than in low latitudes, the largest contributions of ET are observed in Northern America and in Europe, but for R in northern Asia.

HP analysis was also performed for the periods Jan. 2003–Dec. 2009 (Table S2, Figs. S19–S22) and Jan. 2005–Dec. 2011 (Table S3, Figs. S23–S26). No apparent differences were observed, either for the relative contribution of P, ET, and R to TWSC, or in their spatial patterns, compared with the results for the period Jan. 2003–Dec. 2011, suggesting few influences of the choice of study period on our results.

3.3. The relative contributions of precipitation, evapotranspiration, and runoff to TWSC for different climatic regions

We further investigated the relative contributions of P, ET, and R to TWSC in order to explore their impacts under different climate regions (Table S4, Figs. 6 and S27). All basins were classified into 5 group according their corresponding aridity index, such as the arid basins, semi-arid basins, sub-humid basins, humid basins in the mid- and high-latitudes (more than 30° or 30° S) and humid basins in the low latitudes (30° S to 30° N). The largest r^2 values of regression models between TWSC and different P–ET–R combinations were found for basins in sub-humid regions, indicating a high degree of explanation of P, ET, and R to TWSC in these regions. The lowest r^2 values are found in humid basins in mid- and high-latitudes. Except for humid regions in low latitudes where the relative contribution of P was lower than that of ET, the average relative contribution of P, ET, and R can be arrayed as P > ET > R. ET in humid regions was limited mainly by energy rather than by water conditions (McVicar et al., 2012; Rodell et al., 2011; Troy et al., 2011). This may explain the observed larger contribution of ET compared with P in humid basins in low latitudes with high temperature and solar radiation.

Averaging all P–ET–R combinations (Table S4, the largest contribution of P to TWSC was observed in the humid basins of the middle and high latitude, and the smallest contribution was found in arid basins. ET has the largest contribution to TWSC in humid basins of the low latitudes, but presents the lowest contribution in humid basins of the middle and high latitude. The contribution from R is relatively small, and larger value was observed in arid basins.

Shown in the Fig. S28 was the r^2 and the relative contributions of P, ET and R to TWSC in individual basin for different climate areas, respectively. We found that the r^2 and the relative contributions of P, ET and R to TWSC for individual basin were generally consist with the average for different climate areas.

3.4. Relative contributions of precipitation and evapotranspiration to TWSC in some typical basins

To confirm the above findings, we selected six river basins (the Amazon basin, Congo basin, Lena basin, Mississippi river basin, Yangtze basin, and Murray basin) (Fig. 1) to further investigate the relationship between TWSC, P, ET, and R. Fig. 7a-f shows the seasonal cycle of TWSC, P, ET, and R, averaged from all datasets in the six basins. The water balance based $TWSC_{P\text{-}ET\text{-}R}$ was also calculated and compared with GRACE based TWSC. We observed a general coherent seasonal cycle between these two TWSC curves for all the selected basins, suggesting a basic reliability of our result. However, there are also some discernable differences in the variation of TWSC amplitude in some basins, such as for the Lena basin and Murray basin, etc. The differences can be due to

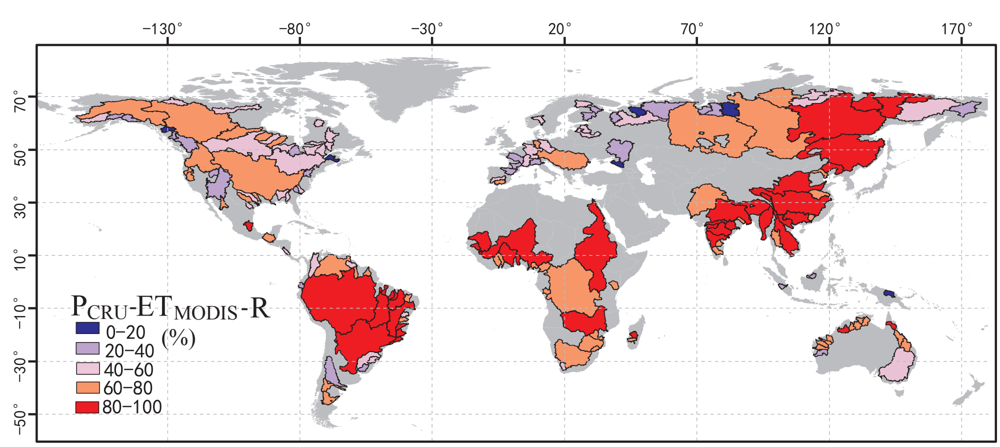

Fig. 4. The global distribution of r^2 of multivariate regression models in global basins based on P_{CRU}–ET_{MODIS}–R dataset combinations.

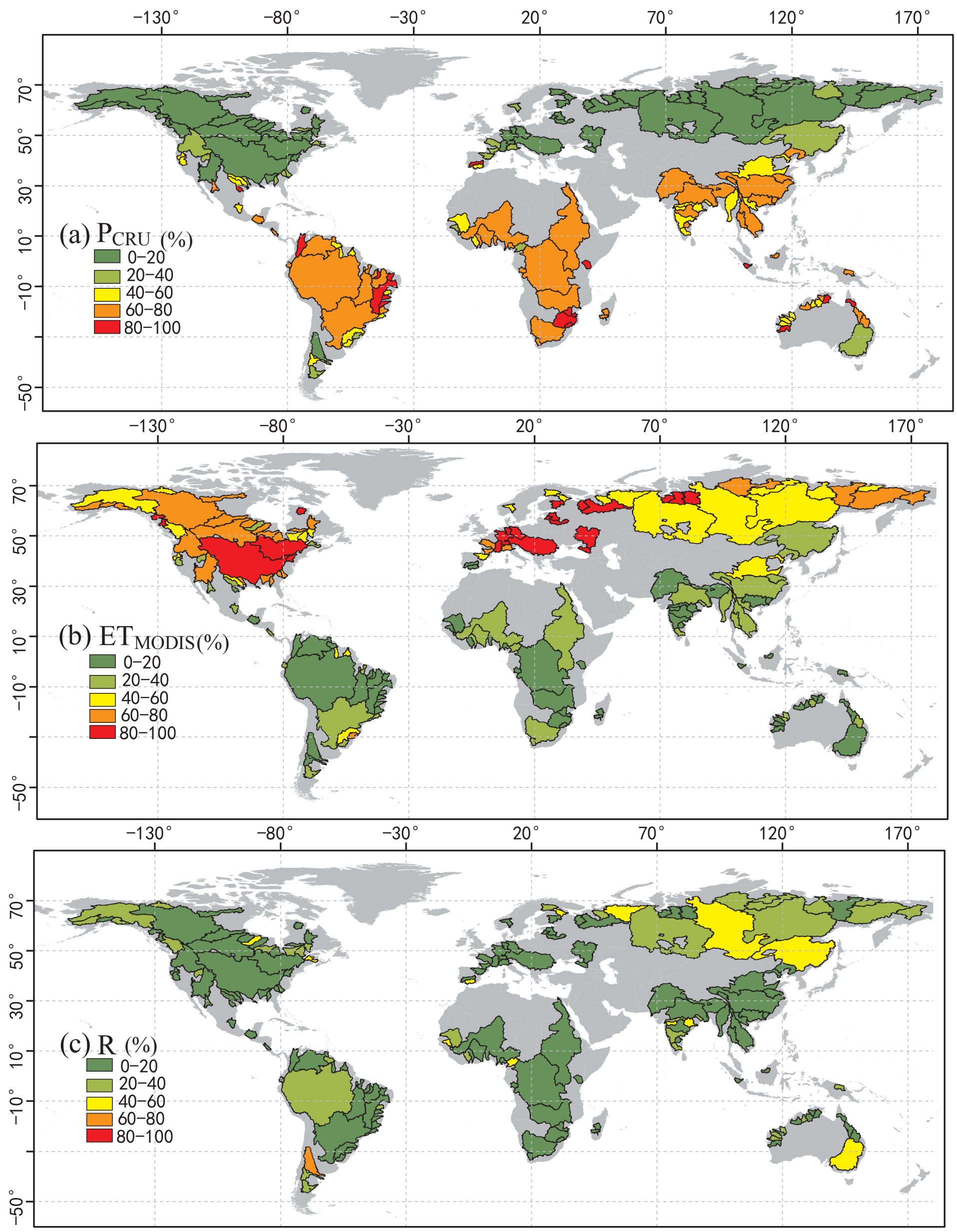

Fig. 5. The global distribution of relative contributions of P_{CRU}, ET_{MODIS}, and R in explaining TWSC.

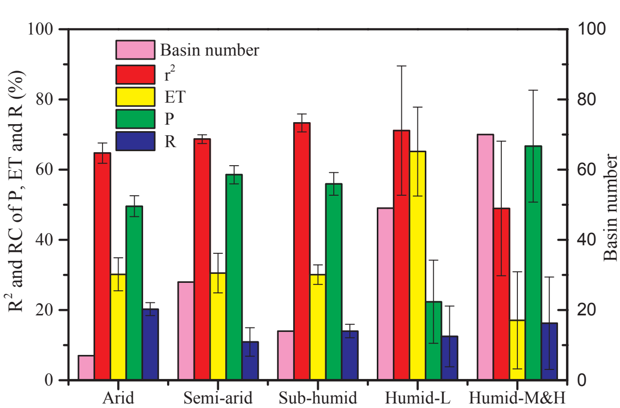

Fig. 6. Average r^2 values and the corresponding relative contributions of P, ET, and R to TWSC in basins under different climate regions. The black bars denote the uncertainties. In addition, Humid-L refers to humid basins in the low latitude areas (30° S to 30° N) and Humid-M&H refers to humid basins in the middle and high latitude (30–90° N and 30–90°S).

several aspects, such as the influence of snowmelt in the Lena basin (Dettinger and Diaz, 2000; Hirschi et al., 2006; Velicogna et al., 2012), the uncertainties in datasets used for the $TWSC_{P\text{-}ET\text{-}R}$ calculation (Soni and Syed, 2015; Syed et al., 2009), etc.

In the Amazon basin (Fig. 7a), according to HP analysis, the relative contributions to GRACE based TWSC were 77.7% ± 2.79% for P, 18.1% ± 3.0% for R, and 4.2% ± 3.1% for ET. This can be confirmed by the higher consistency of the seasonal cycle of TWSC and P, the lower magnitudes of the seasonal cycle for R, and the negligible seasonal change observed for ET. In the Congo basin (Fig. 7b), the seasonal patterns of TWSC, P, and ET are similar, but TWSC seems to be driven mainly by P because of greater magnitude of P. This is consistent with the result of the larger contribution of P to TWSC (71.9% ± 10%) compared with those of ET to TWSC (16.4% ± 4.8%) or of R to TWSC (11.7% ± 5.3%). In the Lena basin (Fig. 7c), we observed an opposite seasonal cycle between TWSC and P/ET/R. In light of previous investigations (Dettinger and Diaz, 2000; Hirschi et al., 2006; Velicogna et al., 2012), the season cycle of TWSC in the Lena basin is highly relied on the runoff peak in the May or June, which was mostly related to the

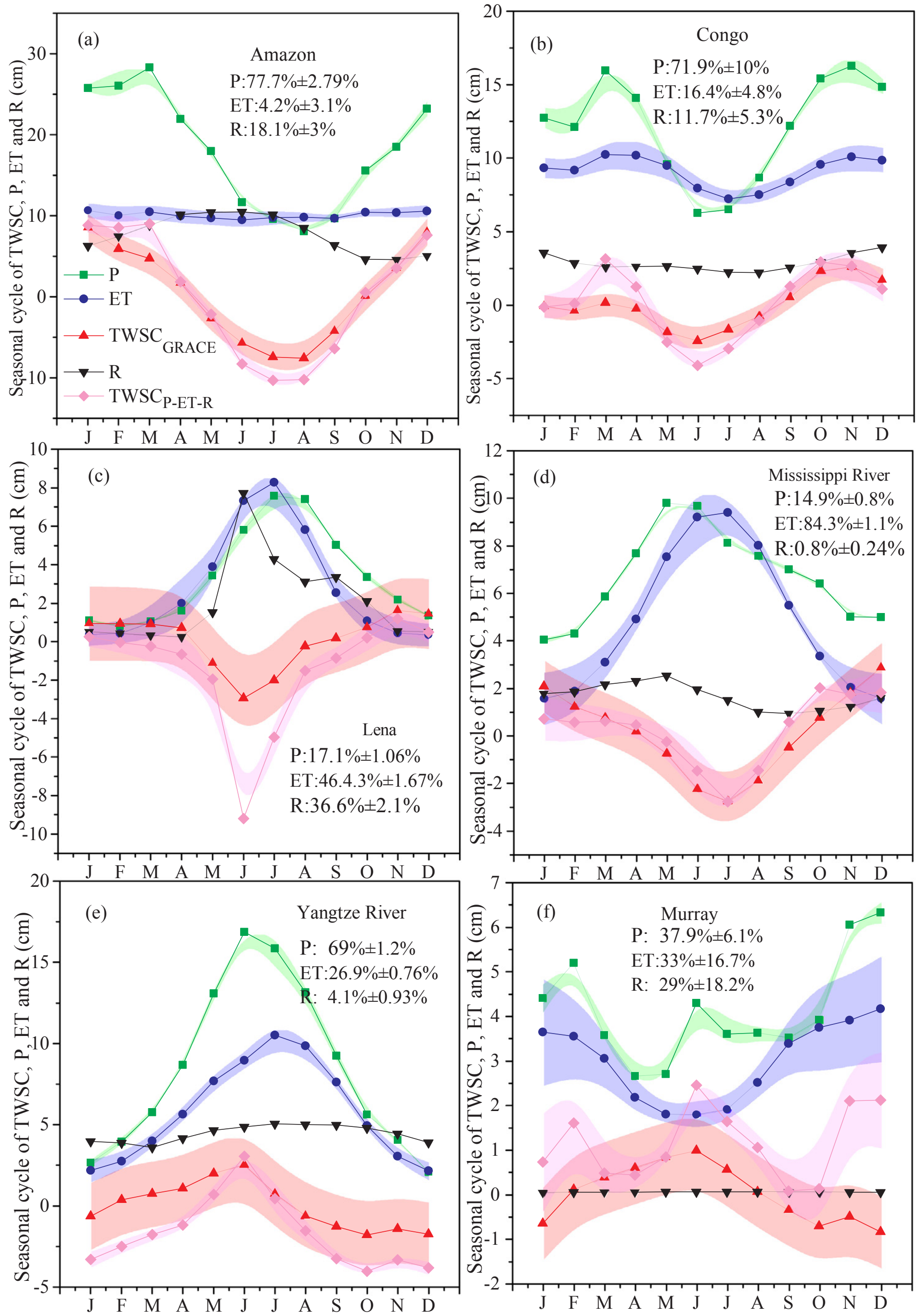

Fig. 7. The seasonal cycles of TWSC, P, ET, and R for six typical basins. Shaded areas indicate the corresponding uncertainties ($TWSC_{GRACE}$ referred to GRACE based TWSC).

snowmelt and runoff. The relative contributions of P, ET and R are 17.1% ± 1.06%, 46.4% ± 1.67% and 36.6% ± 2.1% in this basin, respectively. For Mississippi river basin (Fig. 7d), the lowest value for TWSC corresponding to the highest value for ET occurred in July, implying a dominate influence of ET on seasonal TWSC. This can be confirmed by a 84.3% ± 1.1% contribution of ET on TWSC concluded by this study. Kebede et al. (2014) study suggested that, in this basin, 70% of the yearly rainfall occurred before the growing season, and groundwater extraction for irrigation is needed to meet the crop water need. Irrigation related ET increase may cause the lower TWSC in the summer. In the Yangtze basin (Fig. 7e), TWSC is controlled mainly by P, with a contribution of 69.0% ± 1.2%. In the Murray basin (Figs. 7f, S29), the relative contributions of P, ET, and R were 37.9% ± 6.1%, 33.9% ± 16.7% and 29.0% ± 18.2%, respectively. The peak of GRACE based TWSC occurred in June, corresponding to the lowest ET and a peak of P. There seems to be no seasonal cycle of R. This is because, compared with P and ET, the annual R is very small (0.62 cm/yr) (Hirschi et al., 2006) (Fig. S29). The relative high contribution of R (29.0% ± 18.2%) may be caused by the uncertainty in datasets. We found that different combinations of P-ET-R datasets generate a wide range of values of R's contribution to TWSC (Table S4).

4. Discussion and conclusions

We comprehensively investigated the trends of TWSA and the relationships of TWSC with P, ET, and R for the period of Jan. 2003 to

Dec. 2011 for 168 major river basins in this study. The spatial patterns of trends in TWSA showed good agreement with investigations at global and regional scales (Ahmed et al., 2014; Hassan and Jin, 2016; Mo et al., 2016; Scanlon et al., 2017). Consistent with the results of previous investigations, the TWSA showed the increased trend in the Amazon basin (Chen et al., 2010), in Africa basins such as the Zambezi and Niger (Forootan et al., 2014; Hassan and Jin, 2016; Ramillien et al., 2014), and in Australia basins such as the Lake Eyre and Murray basins (Fasullo et al., 2013). The TWSA increases should be mainly attributed to the increases of precipitation (Han et al., 2019; Long et al., 2017; Reager et al., 2016). In addition, human-induced surface water storage change is also found to promote TWS (Long et al., 2017). For example, the water impoundment of the Three Gorges Reservoir was suggested to increase TWS in the central Yangtze river basin (Long et al., 2015). Decreases in TWSA were observed for 42 basins. Some substantial reductions in TWSA correspond well with regional studies of the groundwater depletion due to the water demand through pumping exceed the water supply through recharge (Scanlon et al., 2012), such as in the North China Plain (Feng et al., 2013; Huang et al., 2015) and the Indus basin in northern India (Chen et al., 2014; Long et al., 2016; Rodell et al., 2009; Tiwari et al., 2009), which indicated the strong impacts of anthropogenic activities. Furthermore, the melting of continuous perennial snow and glacier due to climate warming is also an important driver of TWSA decreases (Chen et al., 2017; Henn et al., 2018; Long et al., 2017). For example, Chen et al. (2017) suggested that the depletion of TWSA for the period 2003–2014 in the upper Brahmaputra River basin may be due to shrinking of the snow and glacier. Similar conditions were also found in some basins in the northern America, such as the Yukon basin and Mackenzie River basin (Jacob et al., 2012; Long et al., 2017).

According to the water balance equation, TWSC should be determined by changes in P, ET, and R, disregarding any disturbances by human activities. P, as the only input flux to the terrestrial water storage, shows a generally positive relationship to TWSC. The influence of P on TWSC could be further attributed to large–scale atmospheric circulation (Reager et al., 2016). For example, a robust positive TWSC–P relationship has been found in ENSO–impacted areas (Fasullo et al., 2013; Sun et al., 2016), such as the Murray basin. ET and R act as a negative flux in the terrestrial water balance, show a negative impact on TWSC, with the most robust impacts being found in mid-and high-latitude basins, such as the Mississippi, Lena and Yenisei basins. These findings are roughly consistent with the results of a global investigation performed by Syed et al. (2008), which explored the drivers of GLDAS based TWSC. Their study suggested that TWSC in high latitudes is forced by snowmelt–runoff, while P dominates TWSC in the tropics, and ET drives TWSC in mid-latitude basins. In contrast to their study, we observed less positive relationships between TWSC and ET and R particularly in low latitudes, which seems to be more reasonable according water balance equation, implying a higher uncertainty of GLDAS based TWSC than that of observed TWSC.

Simple correlation analysis could not represent the true contributions of hydrological fluxes to TWSC. Hence, more importantly, we quantified the relative contributions of P, ET, and R to TWSC using multivariate regression models and HP analysis. Averaging the degree of explanation of 168 basins for all P–ET–R combinations, we found that P, ET, and R explained more than 60% of TWSC, suggesting the dominant influence of the hydrological fluxes to TWSC. This was supported by Reager et al. (2016), which suggested that long–term or large–scale TWSC is controlled mainly by natural factors. In addition, we considered that the remaining (unexplained) may be due to the influences of groundwater withdrawals, return flow, snowmelt, and human activities (Döll et al., 2012). Furthermore, we observed a contrasting pattern of the r^2 between low-and high-latitude basins. The higher values of r^2 are concentrated in several low-latitude basins, such as the Amazon, Nile, Parana, Yangtze, and Congo river basins, whereas relatively low values of r^2 are observed in high-latitude basins. The lower r^2 in some high-latitude basins, such as Yenisei basin and OB basin, might be due to the influence of snowmelt on TWSC (Troy et al., 2011). In addition, some basins, such as the Mississippi basin, experienced strong human activities, and the lower r^2 could be attributed to the groundwater extraction which has not been reflected in the currently used water budget components (Kebede et al., 2014; Zhang et al., 2017).

Furthermore, we observed contrasting patterns in the contributions of P, ET, and R to TWSC between low-and mid-high-latitude basins. In low-latitude basins, especially the tropical basins, P has a larger contribution to TWSC compared with those of ET and R, whereas in mid-high-latitude basins, ET and R has a larger contribution compared with that of P. This pattern is roughly consistent with previous investigations at basin scales. For example, in the tropical Amazon basin, we observed a dominant influence of P on TWSC, and lesser contributions of R and ET, in agreement with the results of Crowley et al. (2008). At the continental scale, we observed that P dominated TWSC in South America and Africa, as previously reported by Liu et al. (2006) and Hassan et al. (2016), respectively.

In particular, our result suggests the largest relative contribution of ET to TWSC are mainly located in basins in the Northern America, such as the Mississippi basin, Columbia basin, Mackenzie basin and Yukon basin, etc. According to previous investigations (Milly and Dunne, 2001; Neal et al., 2002; Walter et al., 2004), in addition to climatological dimension, ET change in some basins strongly influenced by the human activities. For example, in the Mississippi basin, due to the inconformity for the period of rainfall and the crops production, irrigation plays an important role to avoid the crops losses (Kebede et al. (2014). Irrigation practices through groundwater extraction promote the soil water content, and thereby enhance the ET (Ozdogan et al., 2010; Snipes, 2005). This should be the main reason for the large contribution ET to TWSC in this basin. In addition, relative large contribution of R to TWSC are mainly found the northern Asia as reported by Hirschi et al. (2006) and Zhang et al. (2017). Dettinger and Diaz (2000) and Hirschi et al. (2006) referred that the runoff in the northern Asia, such as the Lena basin, Yenisei basin and Volga basin, is mainly generated by the snowmelt.

The results of this study is essential for the understanding of the natural attributions of TWSC and have implications for forecasting TWS dynamics under future climate change. It should be noted that uncertainties still exist. First, multi–sourced datasets of P and ET were used in this study. Although all P–ET–R combinations showed similar capabilities for explaining global TWSC, apparent differences were identified at the scale of climatic regions and basins, indicating the influences of uncertainties between different datasets. The accuracy of products for ET is questioned (Khan et al., 2018; Liaqat and Choi, 2017). Second, the GRDC runoff data suffers from serious data missing in some basins. The reconstructed runoff using a simple linear regression method should inevitably have some uncertainties. In recent years, satellite altimetry technique has been developed to retrieve surface water (Getirana and Peters-Lidard, 2013; Papa et al., 2010; Sneeuw et al., 2014). For example, Sneeuw et al. (2014) estimated runoff using an empirical functional relation between water level estimated by satellite altimetry and the measured runoff at the gauge stations, and suggested this satellite based method outperformed traditional hydrological and hydro-meteorological approach methods. Therefore, satellite altimetry can be applied to fill runoff data in our future studies. Third, we found that P, ET, and R explain only a small proportion of TWSC in several high-latitude basins, implying the influences of snowmelt, groundwater, and permafrost thaw, as reported in previous studies (Döll et al., 2012; Landerer et al., 2010; Syed et al., 2008). Lastly, the lagged effects of P and ET on TWSC were also ignored. For example, the lagged response of TWSC to changes in P in the Amazon basin have been widely reported (Azarderakhsh et al., 2011). These issues are to be considered in our future investigations.

Declaration of Competing Interest

The authors declare that they have no known competing financial interests or personal relationships that could have appeared to influence the work reported in this paper.

Acknowledgments

This work was supported by the Strategic Priority Research Program of the Chinese Academy of Sciences (Grant XDA20060402), the National Key Scientific Research and Development Program of China (Grant 2017YFA0603601), and the National Natural Science Foundation of China (Grant 41671083). GRACE level-2 Mascon solutions produced by NASA's Jet Propulsion Laboratory (JPL) and by the Center for Space Research (CSR) at the University of Texas were obtained from https://grace.jpl.nasa.gov/data/get-data/. Two global precipitation products were obtained from the Climate Research Unit (CRU Time Series v4.00) (http://www.cru.uea.ac.uk/data/) and the Global Precipitation Climatology Centre (GPCC) (https://www.esrl.noaa.gov/psd/data/gridded/data.gpcc.html). Three evapotranspiration (ET) products were obtained from the Moderate Resolution Imaging Spectroradiometer (MODIS) ET product (MOD16A2) (http://files.ntsg.umt.edu/data/NTSG_Products/MOD16/), from simulations produced by Jung and colleagues (Mueller et al., 2013) (https://www.bgcjena.mpg.de/geodb/projects/FileDetails.php), and from the Global Land Data Assimilation System (GLDAS) (https://hydro1.gesdisc.eosdis.nasa.gov/data/GLDAS/). The global digital map of 168 river basins was obtained from Global Runoff Data Centre (GRDC; http://grdc.bafg.de).

Appendix A. Supplementary data

Supplementary data to this article can be found online at https://doi.org/10.1016/j.jhydrol.2019.124194.

References

Ahmed, M., Sultan, M., Wahr, J., Yan, E., 2014. The use of GRACE data to monitor natural and anthropogenic induced variations in water availability across Africa. Earth Sci. Rev. 136 (3), 289–300.
Anderson, R.L., 1942. Distribution of the serial correlation coefficient. Ann. Math. Stat. 13 (1), 1–13.
Andrew, R.L., Guan, H., Batelaan, O., 2017. Large-scale vegetation responses to terrestrial moisture storage changes. Hydrol. Earth Syst. Sci. Discuss. 21 (9), 1–13.
Asoka, A., Gleeson, T., Wada, Y., Mishra, V., 2017. Relative contribution of monsoon precipitation and pumping to changes in groundwater storage in India. Nat. Geosci. 10 (2), 109–117.
Azarderakhsh, M., Norouzi, H., Rossow, W.B., Nasrollahi, N., Khanbilvardi, R., 2011. Inter-annual variation of the total water storage in Amazon and Mississippi river basins for 1984–2006.
Aziz, O.I.A., Burn, D.H., 2006. Trends and variability in the hydrological regime of the Mackenzie River Basin. J. Hydrol. 319 (1), 282–294.
Burn, D.H., Elnur, M.A.H., 2002. Detection of hydrologic trends and variability. J. Hydrol. 255 (1), 107–122.
Chen, J., Li, J., Zhang, Z., Ni, S., 2014. Long-term groundwater variations in Northwest India from satellite gravity measurements. Global Planet. Change 116, 130–138.
Chen, J.L., Wilson, C.R., Tapley, B.D., 2010. The 2009 exceptional Amazon flood and interannual terrestrial water storage change observed by GRACE. Water Resour. Res. 46 (12), 439–445.
Chen, X., Long, D., Hong, Y., Zeng, C., Yan, D., 2017. Improved modeling of snow and glacier melting by a progressive two-stage calibration strategy with GRACE and multisource data: How snow and glacier meltwater contributes to the runoff of the Upper Brahmaputra River basin? Water Resour. Res. 53 (3), 2431–2466. https://doi.org/10.1002/2016wr019656.
Chevan, A., Sutherland, M., 1991. Hierarchical partitioning. Am. Stat. 45 (2), 90–96.
Crowley, J.W., Mitrovica, J.X., Bailey, R.C., Tamisiea, M.E., Davis, J.L., 2008. Annual variations in water storage and precipitation in the Amazon Basin. J. Geod. 82 (1), 9–13.
Döll, P., et al., 2012. Impact of water withdrawals from groundwater and surface water on continental water storage variations. J. Geodyn. 59, 143–156.
Dai, A., 2016. Historical and future changes in streamflow and continental runoff: a review. Terrestrial water cycle and climate change: natural and human-induced impacts. Geophys. Monogr 221, 17–37.
Deng, H., Chen, Y., 2016. Influences of recent climate change and human activities on water storage variations in Central Asia. J. Hydrol.
Dettinger, M.D., Diaz, H.F., 2000. Global characteristics of stream flow seasonality and variability. J. Hydrometeorol. 1 (4), 289–310.
Durbin, J., Watson, G.S., 1971. Testing for serial correlation in least squares regression. III. Biometrika 58 (1), 1–19. https://doi.org/10.1093/biomet/58.1.1.
Fasullo, J.T., Boening, C., Landerer, F.W., Nerem, R.S., 2013. Australia's unique influence on global sea level in 2010–2011. Geophys. Res. Lett. 40 (16), 4368–4373.
Felfelani, F., Wada, Y., Longuevergne, L., Pokhrel, Y.N., 2017. Natural and human-induced terrestrial water storage change: a global analysis using hydrological models and GRACE. J. Hydrol. 553.
Feng, S., Fu, Q., 2013. Expansion of global drylands under a warming climate. Atmos. Chem. Phys. 13 (19), 10081–10094.
Feng, W., et al., 2013. Evaluation of groundwater depletion in North China using the Gravity Recovery and Climate Experiment (GRACE) data and ground-based measurements. Water Resour. Res. 49 (4), 2110–2118.
Forootan, E., et al., 2014. Multivariate prediction of total water storage changes over West Africa from multi-satellite data. Surv. Geophys. 35 (4), 913–940.
Frappart, F., Ramillien, G., Ronchail, J., 2013. Changes in terrestrial water storage versus rainfall and discharges in the Amazon basin. Int. J. Climatol. 33 (14), 3029–3046.
Getirana, A.C.V., Peters-Lidard, C., 2013. Estimating water discharge from large radar altimetry datasets. Hydrol. Earth Syst. Sci. 17 (3), 923–933. https://doi.org/10.5194/hess-17-923-2013.
Gocic, M., Trajkovic, S., 2013. Analysis of changes in meteorological variables using Mann-Kendall and Sen's slope estimator statistical tests in Serbia. Global Planet. Change 100, 172–182.
Han, P., et al., 2019. Improved understanding of snowmelt runoff from the headwaters of China's Yangtze River using remotely sensed snow products and hydrological modeling. Remote Sens. Environ. 224, 44–59. https://doi.org/10.1016/j.rse.2019.01.041.
Harris, I., Jones, P.D., Osborn, T.J., Lister, D.H., 2014. Updated high-resolution grids of monthly climatic observations – the CRU TS3.10 Dataset. Int. J. Climatol. 34 (3), 623–642.
Hassan, A., Jin, S., 2016. Water storage changes and balances in Africa observed by GRACE and hydrologic models. Geod. Geodyn. 7 (1), 39–49.
Henn, B., et al., 2018. High-elevation evapotranspiration estimates during drought: using streamflow and NASA airborne snow observatory SWE observations to close the upper Tuolumne river basin water balance. Water Resour. Res. 54 (2), 746–766. https://doi.org/10.1002/2017wr020473.
Hirsch, R.M., Slack, J.R., 1984. A nonparametric trend test for seasonal data with serial dependence. Water Resour. Res. 20 (6), 727–732.
Hirschi, M., Seneviratne, S.I., Schär, C., 2006. Seasonal variations in terrestrial water storage for major midlatitude river basins. J. Hydrometeorol. 7 (1), 39–60.
Huang, Z., et al., 2015. Subregional-scale groundwater depletion detected by GRACE for both shallow and deep aquifers in North China Plain. Geophys. Res. Lett. 42 (6), 1791–1799.
Humphrey, V., Gudmundsson, L., Seneviratne, S.I., 2016. Assessing global water storage variability from GRACE: trends, seasonal cycle, subseasonal anomalies and extremes. Surv. Geophys.
Jacob, T., Wahr, J., Pfeffer, W.T., Swenson, S., 2012. Recent contributions of glaciers and ice caps to sea level rise. Nature 482 (7386), 514–518. https://doi.org/10.1038/nature10847.
Jung, M., Reichstein, M., Bondeau, A., 2009. Towards global empirical upscaling of FLUXNET eddy covariance observations: validation of a model tree ensemble approach using a biosphere model. Biogeosciences 6 (10), 2001–2013.
Jung, M., et al., 2010. Recent decline in the global land evapotranspiration trend due to limited moisture supply. Nature 467 (7318), 951.
Kebede, H., Fisher, D.K., Sui, R., Reddy, K.N., 2014. Irrigation methods and scheduling in the delta region of Mississippi: current status and strategies to improve irrigation efficiency. Am. J. Plant Sci. 5 (20), 2917.
Kendall, M., 1975. Multivariate Analysis. Charles Griffin Company Ltd.
Khan, M.S., Liaqat, U.W., Baik, J., Choi, M., 2018. Stand-alone uncertainty characterization of GLEAM, GLDAS and MOD16 evapotranspiration products using an extended triple collocation approach. Agric. For. Meteorol. 252, 256–268.
Forootan Khandu, E., Schumacher, M., Awange, J.L., Müller Schmied, H., 2016. Exploring the influence of precipitation extremes and human water use on total water storage (TWS) changes in the Ganges-Brahmaputra-Meghna River Basin. Water Resour. Res. 52 (3) n/a–n/a.
Khandu, K., Forootan, E., Awange, J., Anyah, R., 2015. Impacts of Extreme Climate Events on Total Water Storage (TWS) Changes in Brahmaputra-Ganges-Meghna Basin. Iugg General Assembly.
Landerer, F.W., Dickey, J.O., Güntner, A., 2010. Terrestrial water budget of the Eurasian pan-Arctic from GRACE satellite measurements during 2003–2009. J. Geophys. Res.: Atmos. 115 (D23).
Leblanc, M.J., Tregoning, P., Ramillien, G., Tweed, S.O., Fakes, A., 2009. Basin-scale, integrated observations of the early 21st century multiyear drought in southeast Australia. Water Resour. Res. 45 (4), 546–550.
Liaqat, U.W., Choi, M., 2017. Accuracy comparison of remotely sensed evapotranspiration products and their associated water stress footprints under different land cover types in Korean peninsula. J. Cleaner Prod. 155, 93–104.
Liu, W.T., Xie, X., Tang, W., Zlotnicki, V., 2006. Spacebased observations of oceanic influence on the annual variation of South American water balance. Geophys. Res. Lett. 33 (8), 153–172.
Long, D., et al., 2016. Have GRACE satellites overestimated groundwater depletion in the Northwest India Aquifer? Sci. Rep. 6, 24398.
Long, D., Longuevergne, L., Scanlon, B.R., 2014. Uncertainty in evapotranspiration from land surface modeling, remote sensing, and GRACE satellites. Water Resour. Res. 50

(2), 1131–1151.
Long, D., et al., 2017. Global analysis of spatiotemporal variability in merged total water storage changes using multiple GRACE products and global hydrological models. Remote Sens. Environ. 192, 198–216. https://doi.org/10.1016/j.rse.2017.02.011.
Long, D., et al., 2013. GRACE satellite monitoring of large depletion in water storage in response to the 2011 drought in Texas. Geophys. Res. Lett. 40 (13), 3395–3401.
Long, D., et al., 2015. Deriving scaling factors using a global hydrological model to restore GRACE total water storage changes for China's Yangtze River Basin. Remote Sens. Environ. 168, 177–193. https://doi.org/10.1016/j.rse.2015.07.003.
Longuevergne, L., Scanlon, B.R., Wilson, C.R., 2010. GRACE Hydrological estimates for small basins: evaluating processing approaches on the High Plains Aquifer, USA. Water Resour. Res. 46 (11), 6291–6297.
Luus, K.A., et al., 2013. Modeling the influence of snow cover on low Arctic net ecosystem exchange. Environ. Res. Lett. 8 (3), 1402–1416.
Mann, H.B., 1945. Nonparametric tests against trend. Econometrica: J. Econom. Soc. 245–259.
McVicar, T.R., et al., 2012. Global review and synthesis of trends in observed terrestrial near-surface wind speeds: implications for evaporation. J. Hydrol. 416, 182–205.
Milly, P.C.D., Dunne, K.A., 2001. Trends in evaporation and surface cooling in the Mississippi River Basin. Geophys. Res. Lett. 28 (7), 1219–1222.
Mishra, N.B., Crews, K.A., Miller, J.A., Meyer, T., Millington, A., 2015. Mapping vegetation morphology types in Southern Africa Savanna using MODIS time-series metrics: a case study of Central Kalahari, Botswana. Land 4 (1), 197–215.
Mo, X., Wu, J.J., Wang, Q., Zhou, H., 2016. Variations in water storage in China over recent decades from GRACE observations and GLDAS. Nat. Hazards Earth Syst. Sci. 3 (5), 3251–3286.
Moiwo, J.P., Lu, W., Tao, F., 2012. GRACE, GLDAS and measured groundwater data products show water storage loss in Western Jilin, China. Water Sci. Technol. 65 (9), 1606–1614.
Moiwo, J.P., Yang, Y., Tao, F., Lu, W., Han, S., 2011. Water storage change in the Himalayas from the Gravity Recovery and Climate Experiment (GRACE) and an empirical climate model. Water Resour. Res. 47 (7).
Mu, Q., Zhao, M., Running, S.W., 2011. Improvements to a MODIS global terrestrial evapotranspiration algorithm. Remote Sens. Environ. 115 (8), 1781–1800.
Mueller, B., Hirschi, M., Jimenez, C., Ciais, P., 2013. Benchmark products for land evapotranspiration: LandFlux-EVAL multi-dataset synthesis. Hydrol. Earth Syst. Sci. 17 (10), 3707–3720.
Neal, E.G., Todd Walter, M., Coffeen, 2002. Linking the pacific decadal oscillation to seasonal stream discharge patterns in Southeast Alaska. J. Hydrol. 263 (1), 188–197.
Oki, T., Kanae, S., 2006. Global hydrological cycles and world water resources. Science 313 (5790), 1068–1072.
Ozdogan, M., Rodell, M., Beaudoing, H.K., Toll, D.L., 2010. Simulating the effects of irrigation over the United States in a land surface model based on satellite-derived agricultural data. J. Hydrometeorol. 11 (1), 171–184.
Pan, Y., et al., 2017. Detection of human-induced evapotranspiration using GRACE satellite observations in the Haihe River basin of China. Geophys. Res. Lett. 44.
Papa, F., Durand, F., Rossow, W.B., Rahman, A., Bala, S.K., 2010. Satellite altimeter-derived monthly discharge of the Ganga-Brahmaputra River and its seasonal to interannual variations from 1993 to 2008. J. Geophys. Res. 115 (C12). https://doi.org/10.1029/2009JC006075.
Pokhrel, Y.N., Fan, Y., Miguezmacho, G., Yeh, P.J., Han, S., 2012a. Role of surface water and groundwater on terrestrial water storage variation in the Amazon. J. Hydrol.
Pokhrel, Y.N., Hanasaki, N., Yeh, P., 2012b. Model estimates of sea-level change due to anthropogenic impacts on terrestrial water storage. Nat. Geosci. 5 (6), 389–392.
Ramillien, G., Frappart, F., Seoane, L., 2014. Application of the regional water mass variations from GRACE satellite gravimetry to large-scale water management in Africa. Remote Sens. 6 (8), 7379–7405.
Reager, J., et al., 2016. A decade of sea level rise slowed by climate-driven hydrology. Science 351 (6274), 699–703.
Rodell, M., et al., 2004. Basin scale estimates of evapotranspiration using GRACE and other observations. Geophys. Res. Lett. 31 (20).
Rodell, M., et al., 2018. Emerging trends in global freshwater availability. Nature 557 (7707), 651–659. https://doi.org/10.1038/s41586-018-0123-1.
Rodell, M., Mcwilliams, E.B., Famiglietti, J.S., Beaudoing, H.K., Nigro, J., 2011. Estimating evapotranspiration using an observation based terrestrial water budget. Hydrol. Process. 25 (26), 4082–4092.
Rodell, M., Velicogna, I., Famiglietti, J.S., 2009. Satellite-based estimates of groundwater depletion in India. Nature 460 (7258), 999.
Save, H., Bettadpur, S., Tapley, B.D., 2016. High-resolution CSR GRACE RL05 mascons. J. Geophys. Res. Solid Earth 121 (10), 7547–7569. https://doi.org/10.1002/2016JB013007.
Saylor, J.H., 1992. TQM Field Manual. McGraw-Hill.
Scanlon, B., et al., 2019. Tracking seasonal fluctuations in land water storage using global models and GRACE satellites. Geophys. Res. Lett.
Scanlon, B.R., et al., 2012. Groundwater depletion and sustainability of irrigation in the US High Plains and Central Valley. Proc. Natl. Acad. Sci. 109 (24), 9320–9325. https://doi.org/10.1073/pnas.1200311109.
Scanlon, B.R., et al., 2016. Global evaluation of new GRACE Mascon products for hydrologic applications. Water Resour. Res. 52.
Scanlon, B.R., et al., 2017. Global evaluation of new GRACE mascon products for hydrologic applications. Water Resour. Res. 52.
Schneider, U., et al., 2014. GPCC's new land surface precipitation climatology based on quality-controlled in situ data and its role in quantifying the global water cycle. Theor. Appl. Climatol. 115 (1–2), 15–40.
Sneeuw, N., et al., 2014. Estimating runoff using hydro-geodetic approaches. Surv. Geophys. 35 (6), 1333–1359. https://doi.org/10.1007/s10712-014-9300-4.
Snipes, C.E., 2005. Current agricultural practices of the Mississippi Delta.
Soni, A., Syed, T.H., 2015. Diagnosing land water storage variations in major Indian river basins using GRACE observations. Global Planet. Change 133, 263–271.
Sun, Q., Miao, C., AghaKouchak, A., Duan, Q., 2016. Century-scale causal relationships between global dry/wet conditions and the state of the Pacific and Atlantic Oceans. Geophys. Res. Lett. 43 (12), 6528–6537.
Syed, T.H., Famiglietti, J.S., Chambers, D.P., 2009. GRACE-based estimates of terrestrial freshwater discharge from basin to continental scales. J. Hydrometeorol. 10 (1), 22–40.
Syed, T.H., Famiglietti, J.S., Rodell, M., Chen, J., Wilson, C.R., 2008. Analysis of terrestrial water storage changes from GRACE and GLDAS. Water Resour. Res. 44 (2), 339–356.
Tang, Q., Zhang, X., Tang, Y., 2013. Anthropogenic impacts on mass change in North China. Geophys. Res. Lett. 40 (15), 3924–3928.
Tapley, B.D., 2004a. GRACE measurements of mass variability in the earth system. Science 305 (5683), 503.
Tapley, B.D., Bettadpur, S., Watkins, M., Reigber, C., 2004b. The gravity recovery and climate experiment: mission overview and early results. Geophys. Res. Lett. 31 (9), 4 PP.
Thomas, G., 2006. Evidence for intensification of the global water cycle: review and synthesis. J. Hydrol. 319 (1), 83–95.
Tiwari, V., Wahr, J., Swenson, S., 2009. Dwindling groundwater resources in northern India, from satellite gravity observations. Geophys. Res. Lett. 36 (18).
Tregoning, P., Mcclusky, S., Dijk, A.V., Crosbie, R.S., Peña-Arancibia, J.L., 2012. Assessment of GRACE satellites for groundwater estimation in Australia.
Troy, T.J., Sheffield, J., Wood, E.F., 2011. Estimation of the terrestrial water budget over northern Eurasia through the use of multiple data sources. J. Clim. 24 (13), 3272–3293.
Velicogna, I., Tong, J., Zhang, T., Kimball, J.S., 2012. Increasing subsurface water storage in discontinuous permafrost areas of the Lena River basin, Eurasia, detected from GRACE. Geophys. Res. Lett. 39 (9).
Wahr, J., Swenson, S., Velicogna, I., 2006. Accuracy of GRACE mass estimates. Geophys. Res. Lett. 33 (6), 178–196.
Walter, M.T., Wilks, D.S., Parlange, J.Y., Schneider, R.L., 2004. Increasing Evapotranspiration from the Conterminous United States. J. Hydrometeorol. 5 (3), 405–408.
Watkins, M.M., Wiese, D.N., Yuan, D.N., Boening, C., Landerer, F.W., 2015. Improved methods for observing Earth's time variable mass distribution with GRACE using spherical cap mascons. J. Geophys. Res. Solid Earth 120 (4), 2648–2671.
Wiese, D.N., Landerer, F.W., Watkins, M.M., 2016. Quantifying and reducing leakage errors in the JPL RL05M GRACE mascon solution. Water Resour. Res. 52 (9).
Yang, T., Wang, C., Chen, Y., Chen, X., Yu, Z., 2015. Climate change and water storage variability over an arid endorheic region. J. Hydrol. 529, 330–339.
Yun, P., et al., 2017. Detection of human-induced evapotranspiration using GRACE satellite observations in the Haihe River Basin of China: detecting human-induced ET using GRACE. Geophys. Res. Lett. 44.
Zhang, L. et al., 2017. Validation of terrestrial water storage variations as simulated by different global numerical models with GRACE satellite observations.